Contribution of Ultraviolet and Shortwave Infrared Observations to Atmospheric Correction of PACE Ocean-Color Imagery

-We have evaluated, using simulations with a coupled radiation transfer code, the gain in marine reflectance accuracy expected by including observations in the UV and SWIR compared with just using observations in the visible to NIR.

-The study has been performed for the PACE threshold aggregate bands with respect to the standard MODIS set of bands used to generate ocean color products.

Atmospheric correction methodology

-TOA reflectance (after correction for molecular scattering or not) is decomposed in principal components.

-Components sensitive to the ocean signal are combined to retrieve the principal components of marine reflectance, allowing reconstruction of the marine reflectance.

$$\rho = \rho_{TOA} - \rho_m = f(\rho_w)$$

$$\rho = \sum_i c_{pi} \mathbf{e}_{pi}$$
$$\rho_w = \sum_j c_{wj} \mathbf{e}_{wj}$$
$$c_{wj} = g_j(c_{pi})$$

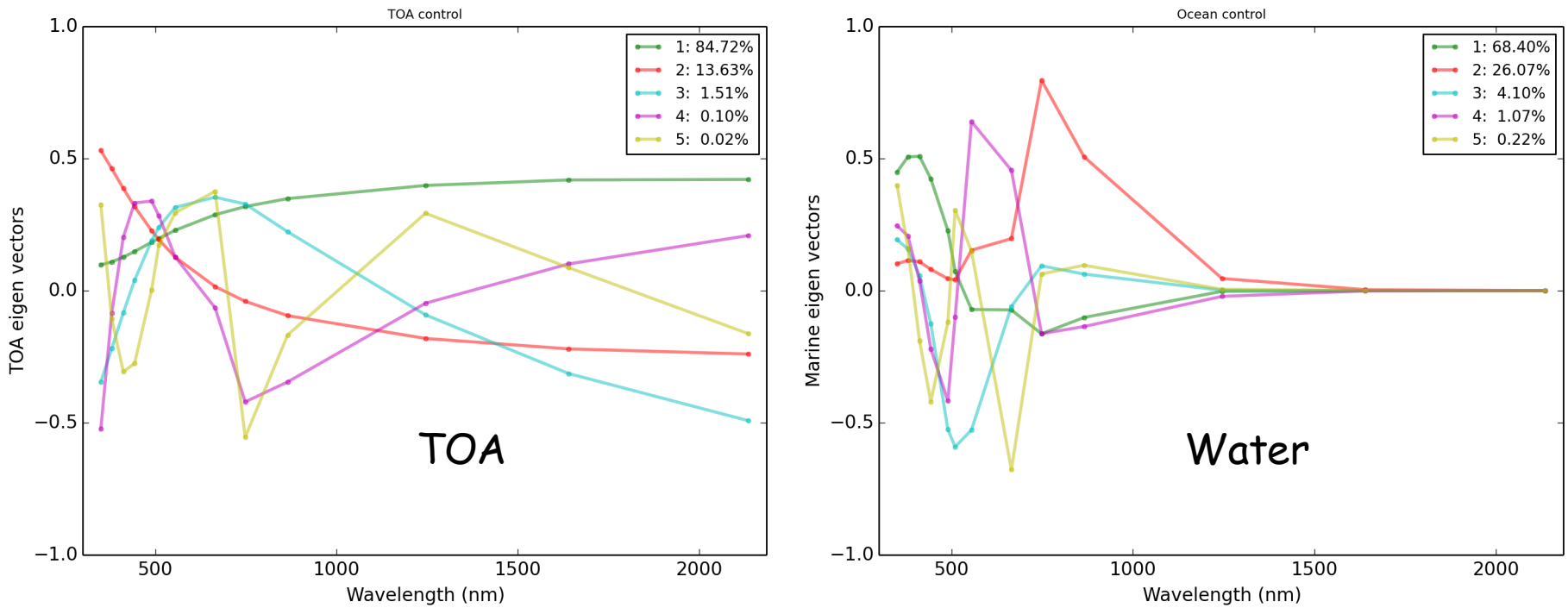

***Figure 1**: Left: The first 5 eigenvectors of the TOA reflectance. Right: the first 5 eigenvectors of the marine reflectance. They were computed for an ensemble of simulations that included a wide range of angular geometries and geophysical conditions (absorbing and non absorbing aerosols, Case 1 and Case 2 waters --Z. Lee), with no noise. Prior distributions are uniform. Spectral bands are centered on 412 ,443, 490, 510, 555, 665, 748, 865, 1245, 1640, and 2135 nm. The first 3 eigenvectors of the TOA reflectance are smooth spectrally and are mostly related to atmospheric/surface processes..*

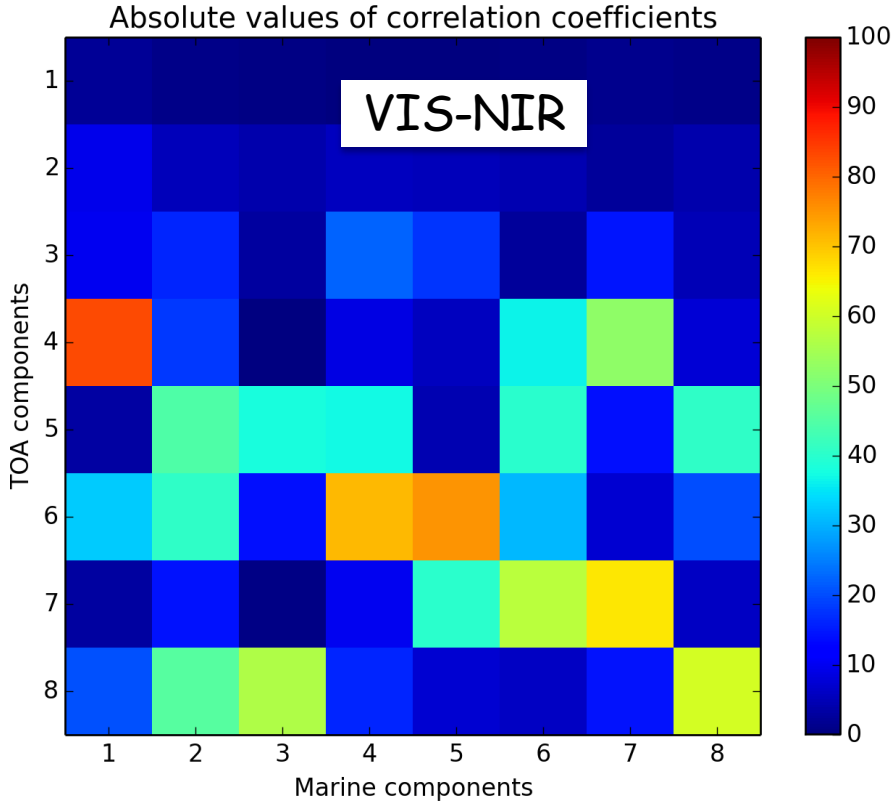

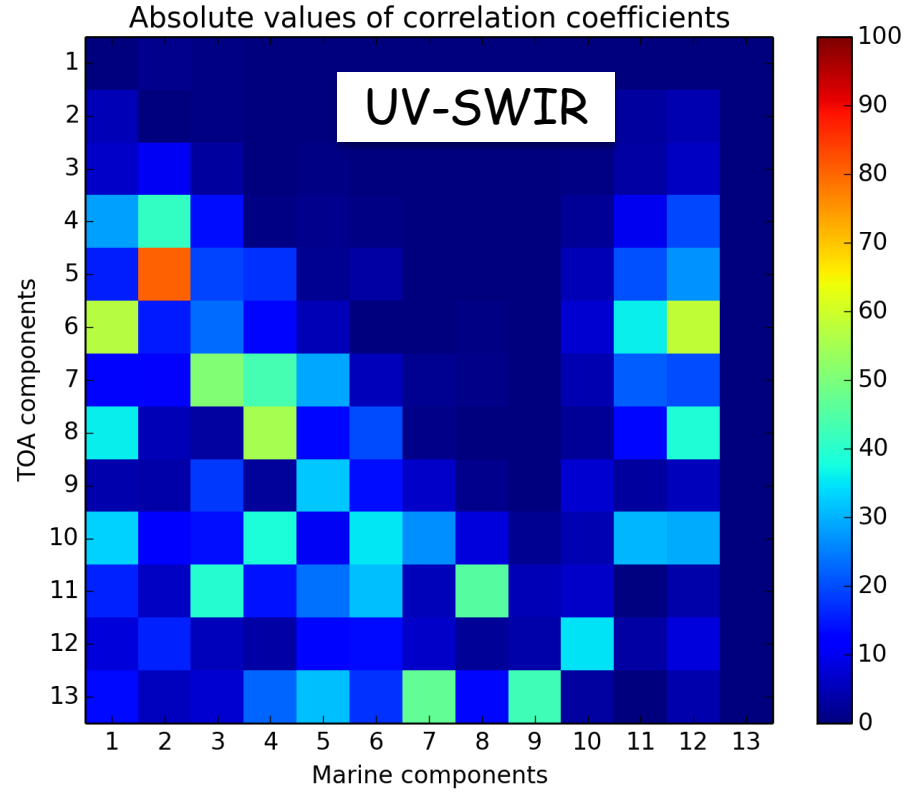

$c_{w1,2} = g_{1,2}(c_{p4}, c_{p5}, c_{p6}, c_{p7})$
$c_{w3,4,5,6} = g_{3,4,5,6}(c_{p5}, c_{p6}, c_{p7})$

$c_{w1,2,3} = g_{1,2,3}(c_{p4}, c_{p5}, c_{p6}, c_{p7}, c_{p8}, c_{p9}, c_{p10}, c_{p11})$
$c_{w4} = g_4(c_{p5}, c_{p6}, c_{p7}, c_{p8}, c_{p9}, c_{p10}, c_{p11})$
$c_{w5} = g_5(c_{p6}, c_{p7}, c_{p8}, c_{p9}, c_{p10}, c_{p11})$
$c_{w6} = g_6(c_{p7}, c_{p8}, c_{p9}, c_{p10}, c_{p11})$
$c_{w7} = g_7(c_{p9}, c_{p10}, c_{p11})$
$c_{w8} = g_8(c_{p10}, c_{p11})$

***Figure 2**: Top: Correlation coefficients (%) between the principal components of ρ, c_{pi}, and the principal components of ρ_w, c_{wj} for standard and PACE bands ; Bottom: Empirical functions based on linear correlation matrix. The mapping is accomplished using neural network modeling. Higher order c_{wj} are fixed at their mean values, estimated on the simulated data ensemble.*

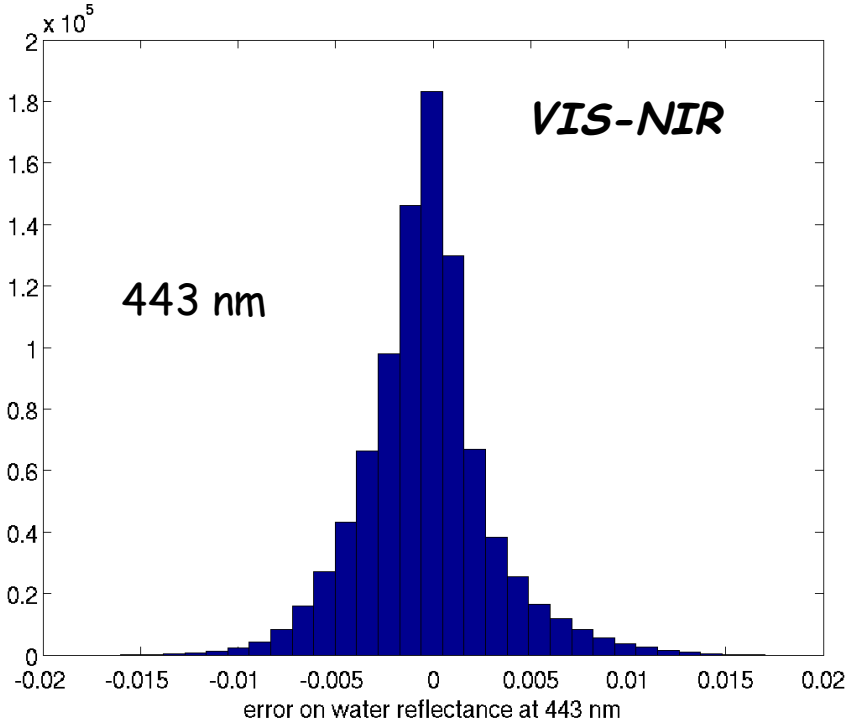

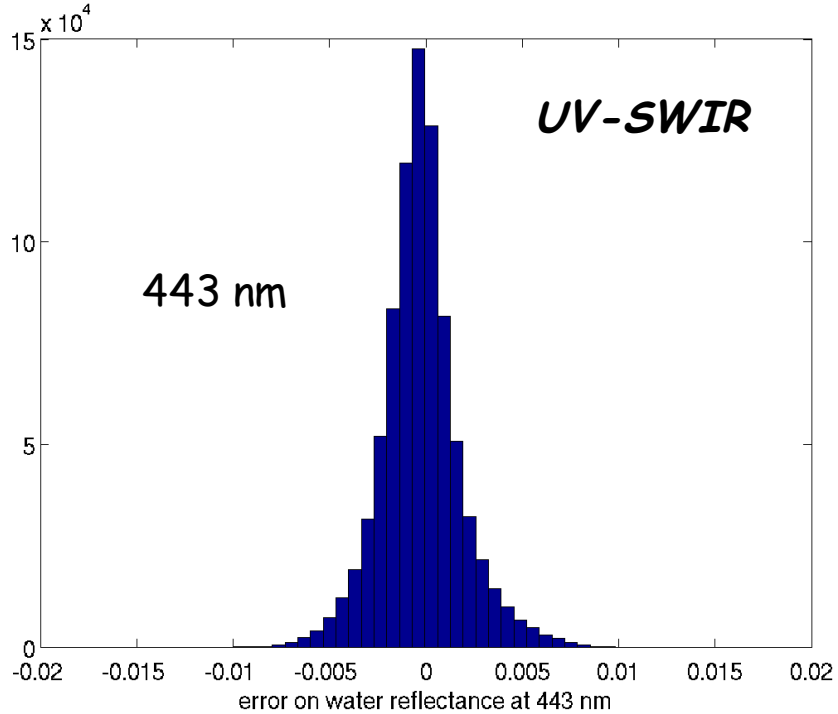

	eRMS	corr(%)	bias
$\rho_w(350)$	0.00238	97	0.00022
$\rho_w(380)$	0.00248	97	0.00029
$\rho_w(412)$	0.00236	98	0.00031
$\rho_w(443)$	0.00204	98	0.00026
$\rho_w(490)$	0.00186	96	0.00020
$\rho_w(510)$	0.00165	93	0.00014
$\rho_w(555)$	0.00158	93	0.00011
$\rho_w(665)$	0.00068	96	0.00007
$\rho_w(748)$	0.00073	96	0.00005
$\rho_w(865)$	0.00043	97	0.00001
$\rho_w(1245)$	0.00006	95	-0.00000

	eRMS	corr(%)	bias
$\rho_w(412)$	0.00373	95	0.00040
$\rho_w(443)$	0.00325	95	0.00037
$\rho_w(490)$	0.00302	91	0.00019
$\rho_w(510)$	0.00258	81	0.00006
$\rho_w(555)$	0.00243	85	0.00016
$\rho_w(665)$	0.00127	94	-0.00009
$\rho_w(748)$	0.00143	99	0.00013
$\rho_w(865)$	0.00098	98	0.00001

***Figure 3**: Theoretical performance of the PCA-based atmospheric correction algorithm. Left: Standard bands; Right: PACE bands. Errors are significantly reduced using the PACE bands.*

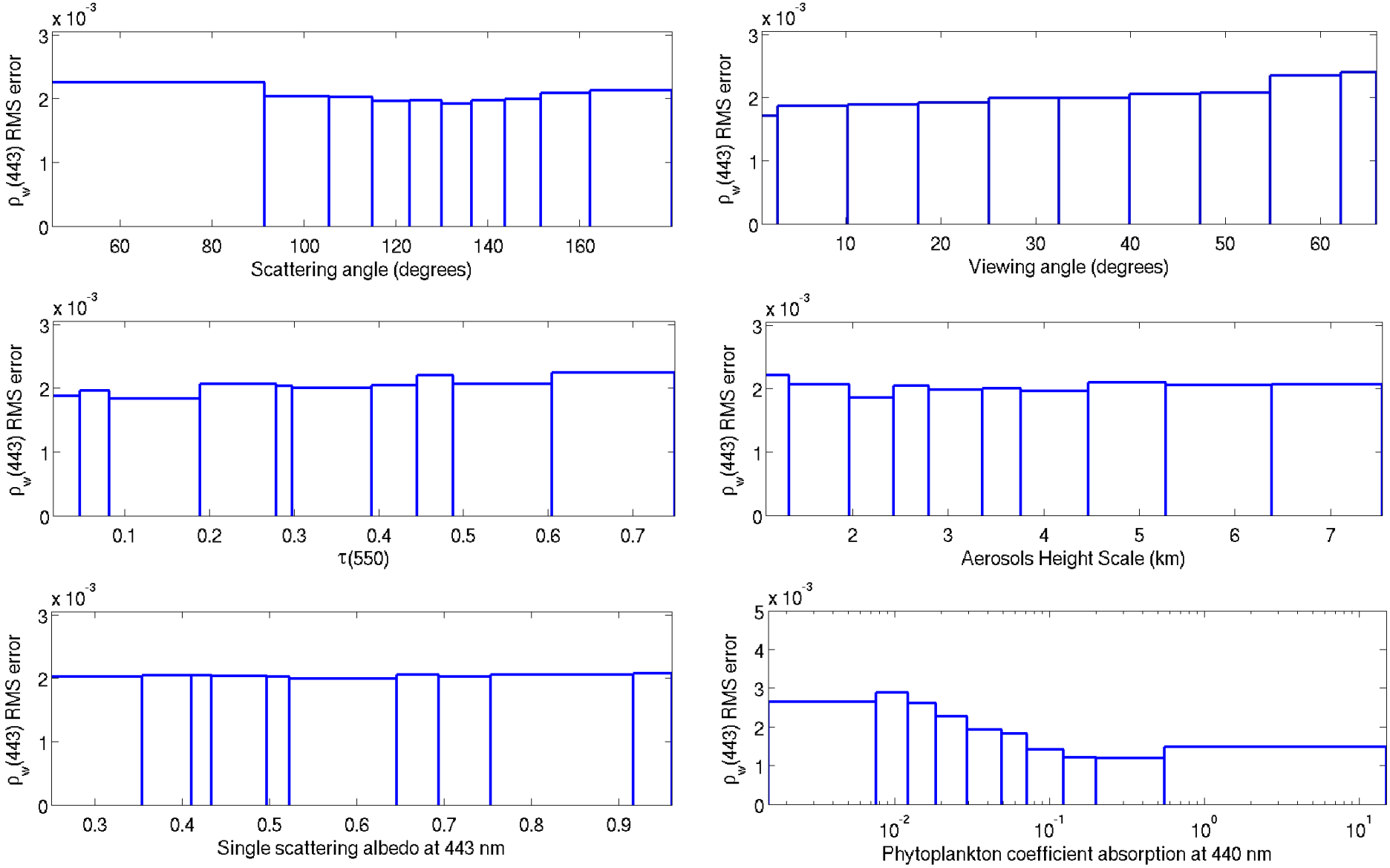

***Figure 4**: Error on retrieved $\rho_w(443)$ as a function of various angular and aerosol parameters. The inversion is performed using the PCA-based algorithm applied to the PACE bands (UV-SWIR).*

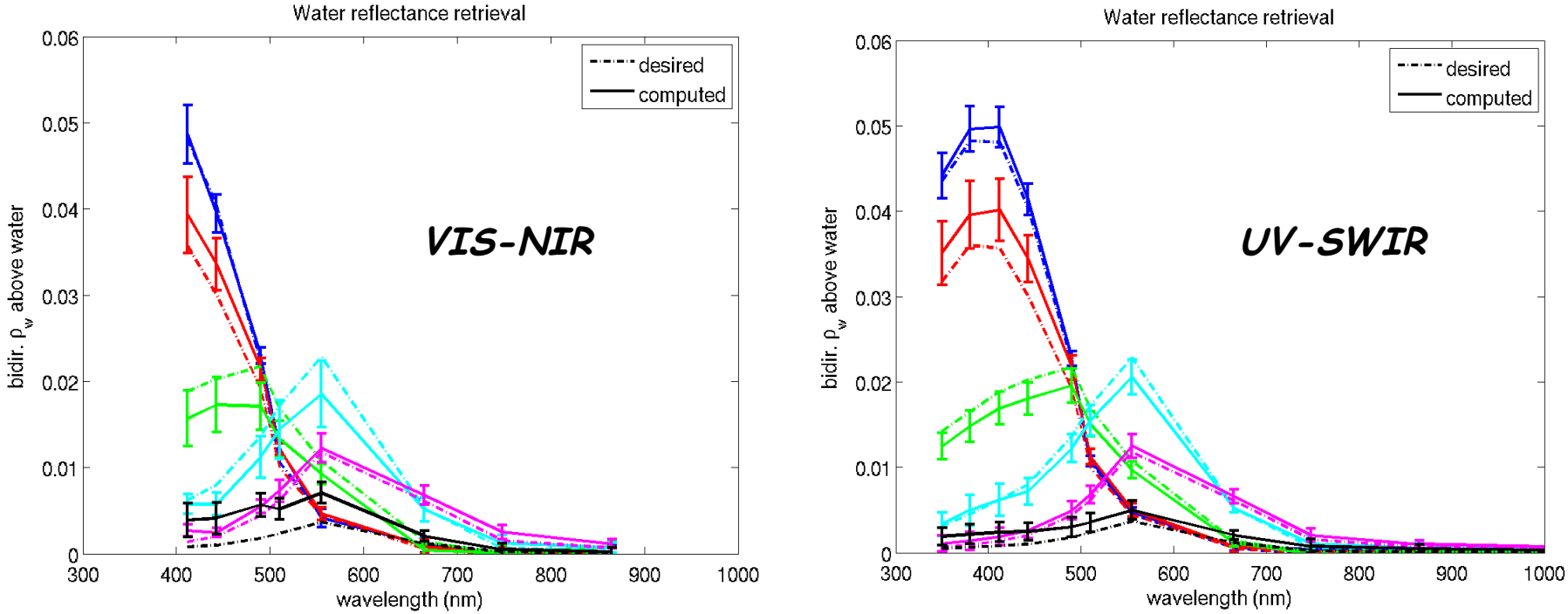

***Figure 5**: Examples of retrieved and prescribed water reflectance spectra. Left: Using the standard bands; Right: Using the PACE bands. Retrievals are generally more accurate using the extended spectral range.*

Summary

-Extending the spectral range of TOA observations to UV and SWIR, retrieval accuracy on ρ_w is improved from 0.037 to 0.0.24 at 412 nm, from 0.0013 to 0.0007 at 665 nm, and from 0.0010 to 0.0004 at 865 nm (Case 2 waters are better handled).

-Performance of the PCA-based algorithm is degraded at large viewing zenith angles and aerosol optical thickness, is better at scattering angles around 120-130 deg., and exhibits little dependence on single scattering albedo and aerosol scale height.

RT Comparisons (plane-parallel versus spherical atmosphere)

AOS-I*: Atmosphere : Rayleigh scattering with AOT=0.5, no depolarization factor, it gives λ = 369.86 nm with AFGL MS and lat.=0., No gaseous absorption. 120 1-km layers. mu_0 =0.6; mu=[0.02,0.10,0.16,0.20,0.28,0.32,0.40,0.52,0.64,0.72,0.84,0.92,1.00]. Monte Carlo, Local Estimation Method, 1 billion photons.

Plane-parallel atmosphere without Sun glint

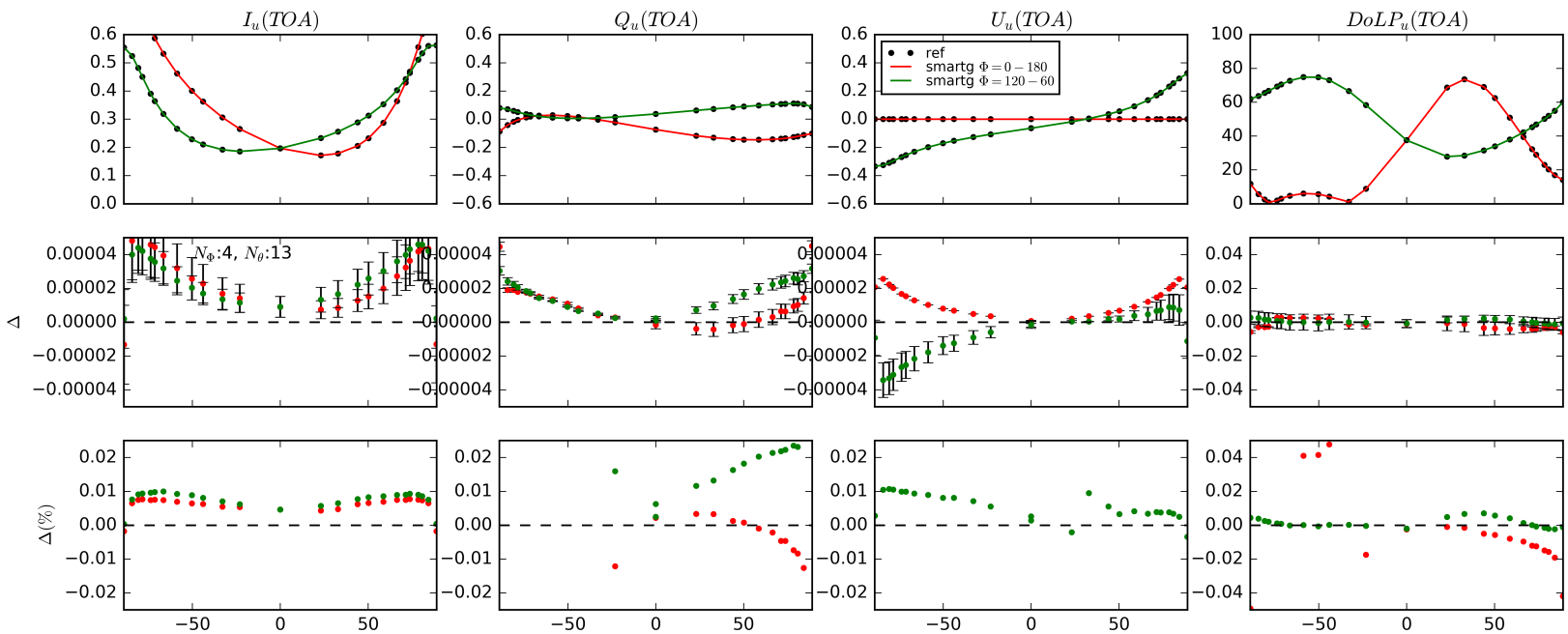

***Figure 6**: Comparison of Stokes parameters computed using the GISS RT code (ref.) and the Monte Carlo code (plane-parallel atmosphere) as a function of view zenith angle for relative azimuth angles of 0, 60, 120, and 180 deg. (red an green curves). Absolute differences are <0.00004 for I, Q, and U, and relative differences are generally <0.02% for DoLP.*

Spherical shell atmosphere without Sun glint

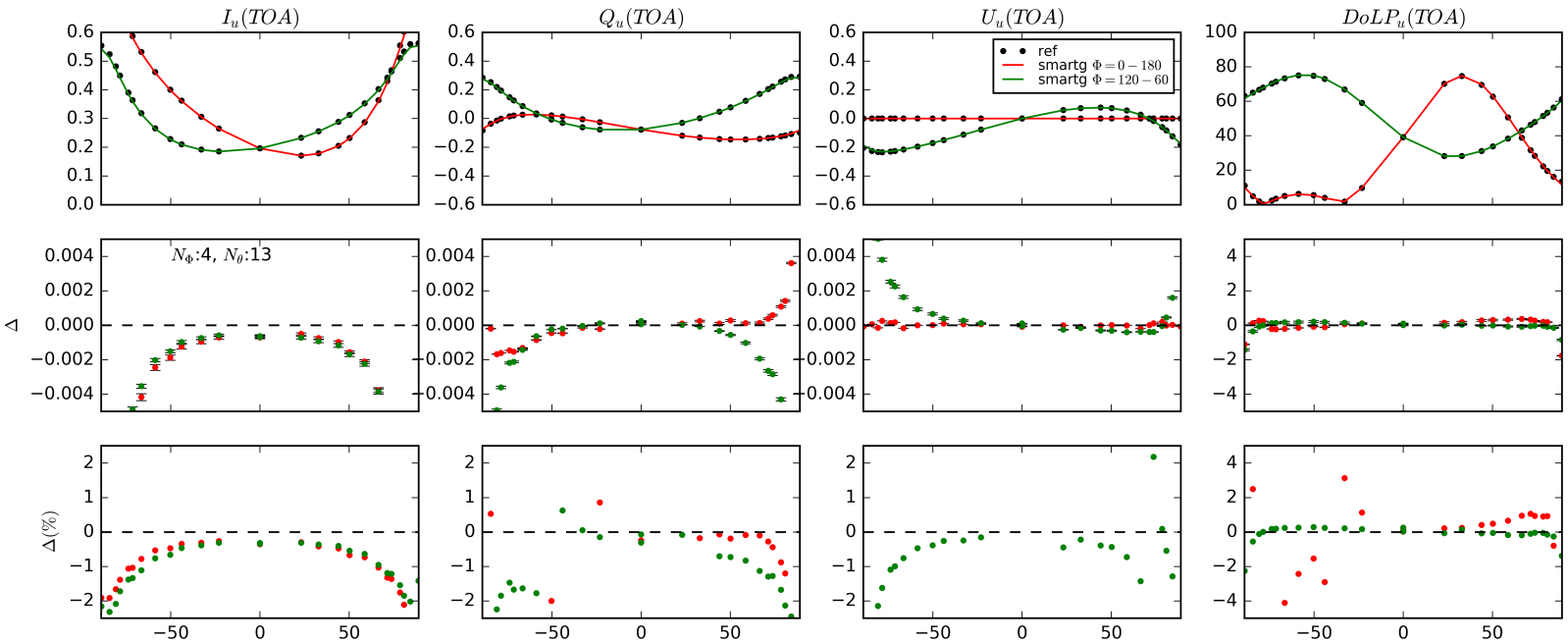

***Figure 7**: Same as Figure 6, but spherical shell atmosphere for Monte Carlo code. The typical effect of sphericity is to lower intensity I by 0.3-0.5% for viewing zenith angles <50 deg. and up to 2% at larger viewing angles, and polarization ratio DoLP by 0.3-0.4%.*

Summary

-Good agreement between results of GISS RT code and Monte Carlo code for AOS-I*. Better agreement can be obtained using more photons.

-Sphericity needs to be taken into account in the calculation of Rayleigh look-up tables for accurate ocean-color remote sensing (as well as temperature profile, index of refraction, depolarization factor of the phase function).